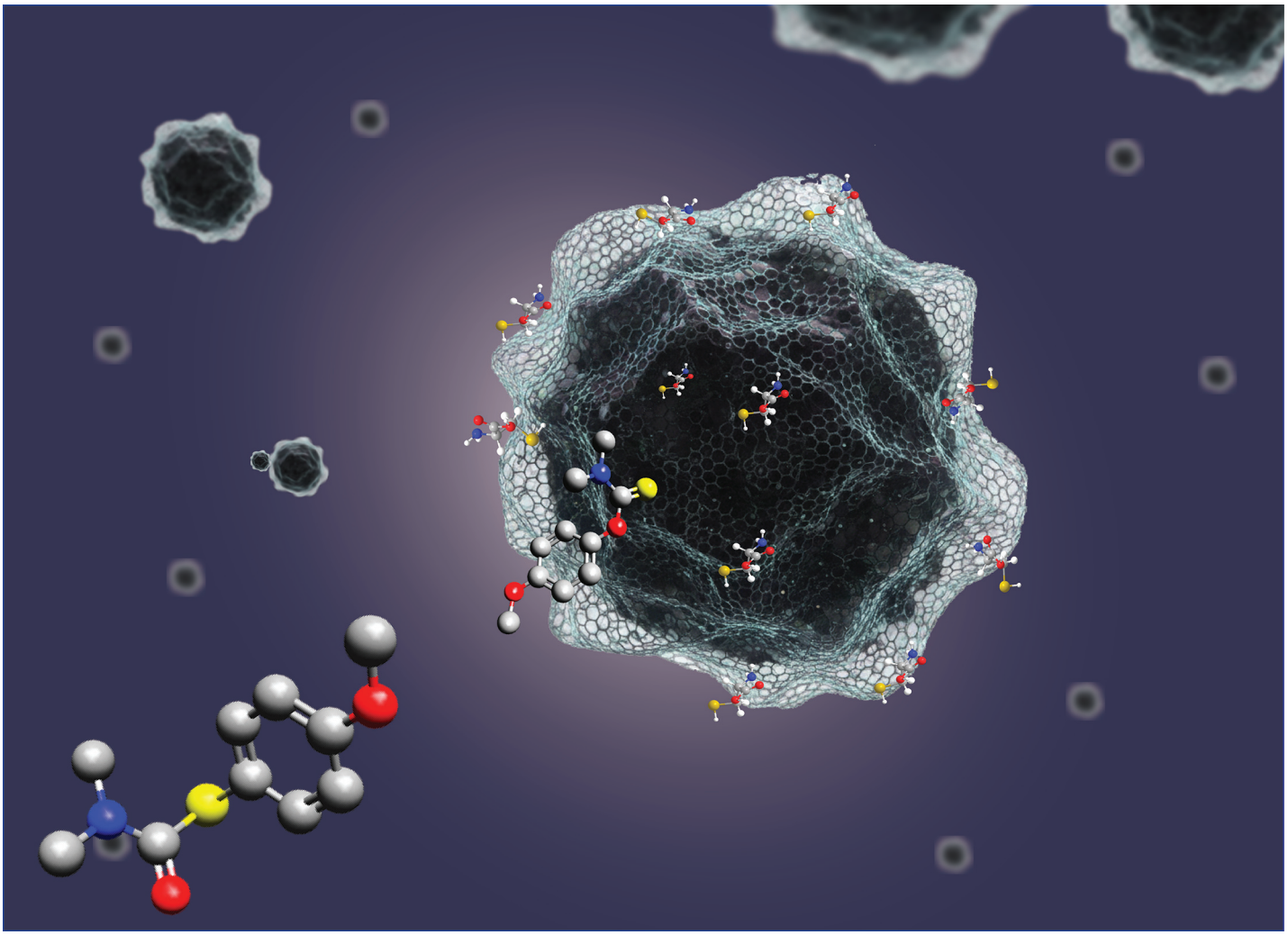

Showcasing research from Professor Mrinmoy De's laboratory, Department of Organic Chemistry, Indian Institute of Science (IISc), Bangalore, India.

Light-driven Newman–Kwart rearrangement under ambient conditions with cysteine quantum dots

The present work features an ambient photo-mediated strategy for the Newman Kwart rearrangement *en route* to electronically diverse *S*-aryl carbamothioates using L-cysteine based carbon quantum dots. The latter serves as a heterogeneous platform, mediating the transformation efficaciously up to at least ten runs. Unlike other methodologies known for this reaction, the current process does not lead to substrate decomposition or side product formation. The strategy, compliant with the various parameters of Green Chemistry, leverages the potential of nanomaterials in synthetic chemistry.

Image reproduced by permission of Mrinmoy De from *Green Chem.*, 2026, **28**, 1542.

Cover artwork partially created using Google Gemini AI.

As featured in:

See Mrinmoy De *et al.*, *Green Chem.*, 2026, **28**, 1542.

ROYAL SOCIETY OF CHEMISTRY

rsc.li/greenchem

Registered charity number: 207890

Green Chemistry

PAPER

View Article Online
View Journal | View Issue

Cite this: *Green Chem.*, 2026, **28**, 1542

Light-driven Newman–Kwart rearrangement under ambient conditions with cysteine quantum dots

Komal Jaiswal, [a] Madhusmita Mahanta[b] and Mrinmoy De *[a]

Received 27th October 2025,
Accepted 1st December 2025

DOI: 10.1039/d5gc05720e

rsc.li/greenchem

The classical Newman–Kwart rearrangement requires harsh reaction conditions (high temperature), resulting in substrate decomposition/side product formation, limiting the scope to electronically deficient substrates to stabilize the anionic transition state in the thermal processes. Thus, it becomes imperative to develop milder protocols for this reaction. The immense potential of nanomaterials as dynamic heterogeneous catalysts, coupled with the scope of photo-mediated transformations, provides a unique opportunity to tackle this challenge. In continuation of our efforts to develop the field of nanomaterial-mediated photocatalysis, we fabricated carbon dots as nanocatalysts to mediate the reaction under ambient temperature and a very short reaction time. Our method was more compatible with electron-rich substrates, corroborating the operation of a cationic mechanism. Interestingly, electronically neutral (and to some extent, electronically poor) substrates were also facile participants in the reaction, showing the robustness and uniqueness of the system in contrast to existing methods. The material could retain its activity for up to ten runs and was compliant with the various parameters associated with a green protocol. This study exemplifies the potential of nanomaterials in mediating otherwise critical synthetic strategies.

Green foundation

1. We present a sustainable, efficient and simple strategy for NKR, photocatalysed by Cysteine-based quantum dots. The economical, single-step preparation of the robust, recyclable catalyst and the compatibility of the reaction with various factors significant for a green approach are the highlights of this work.
2. The estimation of the Green Chemistry metrics highlights the efficient and benign nature of the protocol in terms of minimal waste generation, closeness of the 'ideal' design and practical execution of the reaction (*via* a simple *modus operandi*). These values include environmental factor (*E*-factor): 0.02, reaction mass efficiency (RME): 97.99%, atom economy (AE): 100%, optimum efficiency (OE): 97.99%, and EcoScale score: 83.
3. The work can be made greener by switching completely to the use of water as the solvent, which, however, is challenging, considering the issues of solubility, side product formation, possibility of photo-mediated water splitting processes and so on. These studies are currently ongoing in our laboratory.

Introduction

The Newman–Kwart rearrangement (NKR) is considered to be a highly relevant transformation, allowing the conversion of a diverse range of phenols to thiophenols (Scheme 1a).[1,2] In the reaction scheme, the phenol initially undergoes conversion to the *O*-aryl carbamothioate, which further takes part in the intramolecular NKR step involving the aryl migration to generate the *S*-aryl carbamothioate, driven by the thermodynamically favored conversion of C=S to C=O. Finally, a reduction process generates the thiophenol analogue. In addition, the desulfurization of the thiophenols can provide access to various arenes, starting from the phenols.

A typical thermal NKR process involves an intramolecular aromatic nucleophilic substitution reaction. The rearrangement step is believed to involve a zwitterionic four-membered spirocyclic transition state (TS), formed in a concerted manner. Access to this TS essentially requires a high enthalpy of activation, and consequentially, the initial reports for NKR relied on the use of very high reaction temperatures.[3] Considering the anionic nature of the TS, electron-withdrawing groups (EWGs) on the aryl ring were found to be more compatible under the classical reaction conditions (Scheme 1b). However, the elevated temperatures often resulted in substrate decomposition and side product formation.

In general, suitable *ortho*-substituents may enhance the rate (this is attributed to the rotational restriction around the Ar–O bond; Ar: aryl); however, double *ortho* substituents or sterically encumbered species fail to undergo the rearrangement.[4] The reaction is proposed to obey first-order

[a]*Department of Organic Chemistry, Indian Institute of Science, Bangalore-560012, Karnataka, India. E-mail: md@iisc.ac.in*
[b]*Department of Chemistry, Indian Institute of Science Education and Research, Tirupati-517619, Andhra Pradesh, India*

a) General procedure for conversion of phenols to thiophenols:

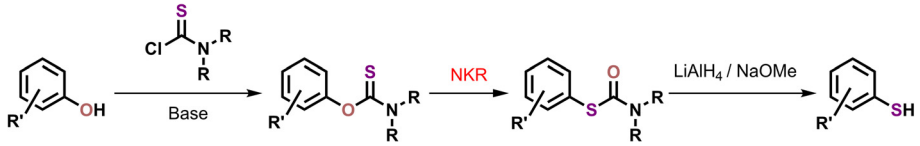

b) Previous reports:

Thermal NKR:

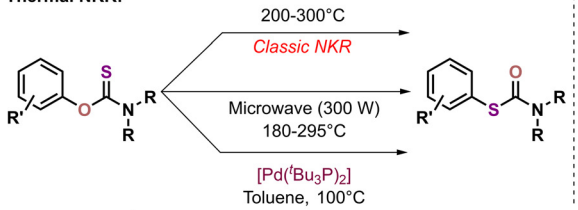

Mechanism for classical NKR:

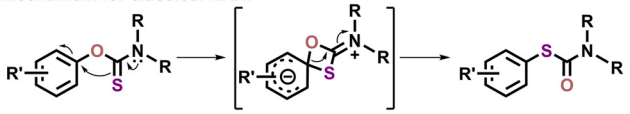

- *High temperature*
- *Limited scope/functional group tolerance*
- *Side product formation*
- *Substrate decomposition*

Photocatalytic NKR:

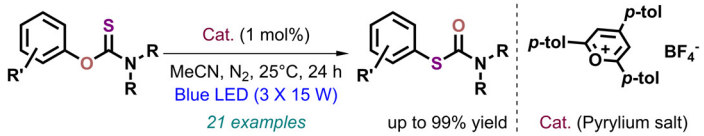

- *Complex catalyst preparation (overall 31% yield)*
- *Restricted diversity among the functional groups*
- *Unrecyclable catalyst*
- *First photocatalytic protocol under ambient conditions*

c) This work:

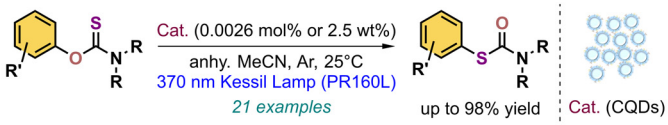

- *Facile access to CQDs without any capping agent/stabilizer*
- *Ambient condition NKR with broad scope*
- *No substrate decomposition*
- *No side products*
- *Sustainable and fully recyclable catalyst*
- *Low catalyst loading*
- *Ideal Green Chemistry metrics*

d) Comparative analysis: this work vs. previous reports:

Parameter	This work	Previous reports
Temperature	25°C	25 (photo-based) to >280 (thermal)°C
Catalyst preparation	Single step, no purification, high yield, economical; overall green process using H_2O as solvent	Either expensive commercially available metal-based systems or prepared in the laboratory, but with a low overall yield
Catalyst performance	Robust and active even at low loadings, easily separable from the reaction mixture, reusable in multiple reaction cycles (atleast 10 runs) without any compromise with the activity	Inseparable from the reaction mixture and not reusable in subsequent runs of the reaction
Efficiency of the strategy	Highly atom economic process due to absence of side product or substrate decomposition	Side product or substrate decomposition common due to harsh reaction conditions
Environmental hazard and ease of process execution	Non-hazardous and environmentally compatible ingredients; strategy and components easy to handle and execute	Metal-based catalysts are inherently associated with toxicity, bio-accumulation/magnification and disposal issues
Energy efficiency	Highly efficient protocol relying on light as the source of catalyst activation with low reaction times	High temperature requirements overpowers the sustainability aspect of energy consumption
Reaction Mass Efficiency (RME)	97.99%	~95% (photo-based process)
Optimum Efficiency (OE)	97.99%	~95% (photo-based process)

e) Estimation of EcoScale value

Parameters considered (taking the model reaction): yield, cost, safety, technical setup, temperature, time, workup/purification protocol
Penalty points: 17
EcoScale Value: 83, implying an excellent synthetic strategy

Scheme 1 (a) Schematic overview of the transformation of phenols to thiophenols, mediated by NKR; (b) known methodologies for NKR *via* the thermal or photo-mediated pathways; (c) the current work on carbon quantum dots (CQDs) NKR driven by light; (d) comparative analysis of this work with the known methods for NKR and (e) EcoScale value based on economical/ecological parameters.

kinetics, as also demonstrated by Miyazaki.[5] The TS is expected to be more stable in the case of polar solvents, although there has not been much investigation in this regard.[6]

Over the years, researchers have come up with multiple variations of the classical NKR, as depicted below (Scheme 1b).[1,7,8] Gilday and co-workers developed a microwave-based synthetic route to access the *S*-aryl carbamothioates, wherein the

electron-rich *O*-aryl carbamothioates required elevated temperatures as compared to their electron-deficit counterparts. The temperature requirement was partially relaxed in another protocol, as demonstrated by Renny *et al.*, using a low-valent Pd-based system that was capable of inserting in the Ar–O bond.

Recently, Nicewicz's group developed the pyrylium photocatalyst for ambient temperature NKR proceeding *via* a radical cationic pathway (Scheme 1b).[9] This protocol allowed for the extension of NKR to electronically rich substrates as well. The strategy involved a single electron transfer (SET) process based on the *in situ O*-to-*S* aryl migration observed in electron spray ionization mass spectrometry (ESI-MS) studies of *O*-aryl carbamothioates.[10] Although the aforesaid protocol was a major breakthrough in this field, providing the scope to harness the efficiency of light for mediating complex strategies, the preparation of the photocatalyst was a challenging step with the overall yield being only 31% (relative to the precursor). The scope of the reaction did not cover the substrates having electron-withdrawing substituents, or those which did not have any substitutions at all. Moreover, the catalyst was inseparable from the reaction mixture, highlighting the need for further expansion and development of sustainable catalytic systems for this critical, yet highly relevant transformation. Additionally, carbon-black[11] and TiO_2 [12]-based systems have been explored for photo-mediated NKR, although they too have some limitations.

Over the last few years, carbon-based materials have evolved significantly for myriads of applications. The discovery of carbon nanotubes (CNTs) in 1991 leveraged the development of this class of nanomaterials and graphene occupied the limelight due to its high conductivity, carrier mobility and other properties.[13,14] Fullerenes,[15] graphene,[16,17] nanodiamonds,[18] CNTs[19] and carbon dots (CDs)[20] are some of the broad classes of carbon-based nanomaterials. The modification of the surface functional groups is a common method for tuning the properties of these materials. Additionally, they are relatively less toxic as compared to other nanomaterials, which has allowed for their potential usage in biomedical fields.

CDs are quasi-lower-dimensional, photoluminescent entities with high quantum yield and sizes of mostly around 20 nm (discovered accidentally during the purification of CNTs in 2004). CDs are sub-classified as graphene quantum dots/QDs[21,22] (GQDs: mono- or multi-layered graphite structures on the surface/edge; π-interactions dictate the optical properties; prepared mostly *via* top-down methods), carbon QDs[23,24] (CQDs: spherical entities, obtained *via* bottom-up approaches such as cross-linking, assembling, carbonization, polymerization, *etc*. from small molecules; they exhibit photoluminescence due to quantum confinement) and carbonized polymer dots[25] (CPDs: extensively cross-linked, assembled, spherical, structures with a core–shell stable arrangement; the core has dehydrated/cross-linked polymers, while the shell bears ample functional groups). The molecular structure and crosslink-enhanced emission effect account for the photoluminescence of CPDs, which is in stark contrast to GQDs and CQDs.[24]

CDs exhibit strong absorption in the UV-region and a tail in the visible region.[26] These arise from the π-to-π* (C=C) or n-to-π* (C=O or C=N) transition.[27,28] The π-conjugated electrons from the sp^2 centres can also result in emission in the near-infrared (NIR) zone.[29] Generally, CDs prepared by bottom-up approaches bear a higher quantum yield as compared to those prepared by top-down methods. This implies that CQDs and CPDs have higher quantum yield than GQDs. Additionally, CDs show an excitation-dependent emission profile arising from the various centres exhibiting photoluminescence, as well as the differently-sized particles in a given system.[28,30] The C=O or C=N moieties may also contribute to room temperature phosphorescence *via* strong spin–orbit coupling, while doping with heteroatoms or halogens can favour the n-to-π* transitions in these bonds, promoting intersystem crossover.[31–33] CPDs are more likely to show phosphorescence due to a rigid matrix comprising the covalently crosslinked framework, which can reduce the extent of non-radiative transitions.[34]

CDs have been employed for sensing (chemical and biological analytes),[34,35] catalysis (in water-splitting, HER, OER, ORR mostly and a few synthetic transformations),[36–39] device (*e.g.*, LEDs, solar cells, and batteries)[40–42] fabrication, bioimaging,[43] phototherapy,[44] and drug delivery applications.[45] As an example, Jayamurugan and co-workers used sulfonic acid-functionalized CDs for the synthesis of 5-hydroxymethylfurfural and ethyl levulinate from *p*-toluenesulfonic acid.[46] Furthermore, they reported the multifunctional Fe-doped sulfonic acid-functionalized CDs for the synthesis of 5-hydroxymethylfurfural and furfural.[47] Despite these developments, the advances in the field are still considered to be in a nascent stage as compared to other nanomaterials, paving the way for further application and structure-oriented research in this sector.

During the initial phase of our investigations to design a benign strategy for NKR, we had used other nanomaterials, such as transition metal dichalcogenides (TMDs), primarily considering our past interest in the use of TMDs as photocatalysts for various reactions.[48–52] We screened various nanosheets/QDs (to check the effect of dimensionality), and found that although MoS_2 QDs worked for NKR of substrate **1a** which had an electronically rich substituent, the yield was very poor. We then modified the TMD material using metal dopants (Fe, Co and Ni) as well as various ligands (3-mercaptopropionic acid and L-cysteine) to tune their band alignments and surface chemistry, respectively. Additionally, we used composites of MoS_2 with other nanomaterials such as CdSe. Despite numerous trials, none of the tailored catalytic platforms (subjected to various reaction parameters) provided any improvement for the NKR process (SI, section 3). We concluded that TMDs were not a suitable class of nanomaterials for this transformation. Considering the popularity of CDs in multitudes of applications as discussed before, we were tempted to test their efficacy as photocatalysts. The CDs were

prepared using a hydrothermal process without the induction of any external capping agent/stabilizer. We envisaged that the fluorogenic CQDs could be suitably tuned for NKR, and subsequent optimizations could lead us to an optimal strategy (Scheme 1c). Indeed, our method worked well under ambient reaction conditions for the conversion of a wide range of *O*-aryl carbamothioates to the corresponding *S*-aryl carbamothioates, with substituents which were electronically rich (very short reaction time), deficient or neutral. This was a major achievement of the designed strategy in contrast to the existing reports, considering its generality to accommodate electronically diverse substrates. The CQDs showed no loss in catalytic efficacy even after ten runs of NKR, highlighting its robust nature and further exemplifying its potential as sustainable mediators of organic transformations, particularly with respect to the design of specifically tailored catalysts for relevant synthetic processes.

The comparison of our results with literature reports led us to the conclusion that the as-designed and developed strategy was not only compatible (and even better than the known methods) with the multiple metrics in green chemistry,[53] but was also environmentally non-hazardous and easily executable (Scheme 1d). This was substantiated with the estimation of the EcoScale value,[54] and the final score exemplified the suitability of the strategy in keeping with the principles of green chemistry (Scheme 1e).

Results and discussion

Preparation and characterization of cysteine CQDs

The CQDs were prepared from L-cysteine as the precursor. The commercially available starting material was subjected to hydrothermal treatment at 200 °C, causing it to break down into smaller dimensional analogues (Fig. 1a). The preparation procedure did not require the incorporation of any additional capping agent or stabilizer. The synthesized CQDs are sticky in nature due to the presence of no capping agent/functionalities. After the preparation, the nanomaterial was characterized by various optical and microscopic techniques.

During the TEM (transmission electron microscopy) imaging, spherical particles were observed. Each spherical domain had a size of around 20 nm and many such domains were present in close proximity to one another in the form of a network (Fig. 1b). This observation was further substantiated by the DLS (dynamic light scattering) studies, wherein the hydrodynamic diameter was found to be much larger than expected for individual nanoparticles of size ~20 nm (SI, Fig. S1). The absence of any capping agent may be responsible for the close proximity, yet there is the distinct presence of such dots. Additionally, the molecular weight of the CQDs was estimated to be 211.9 kDa from the SLS (static light scattering) method (SI, Fig. S2).

The optical properties of the nanomaterial were recorded to evaluate their photochemical features. As expected, in the UV-visible absorption profile, the n-to-π* (C=O) transition resulted in a maxima in the UV region around 370 nm, while no peak was observed in the visible region in the absorption profile of the CQDs (Fig. 2a).[20] The fluorescence profile exhibited an excitation-dependent emission behaviour, in line with the previous reports, highlighting the polychromophoric nature of the nanomaterial, which results in multiple photoluminescent centres (Fig. 2b).[20]

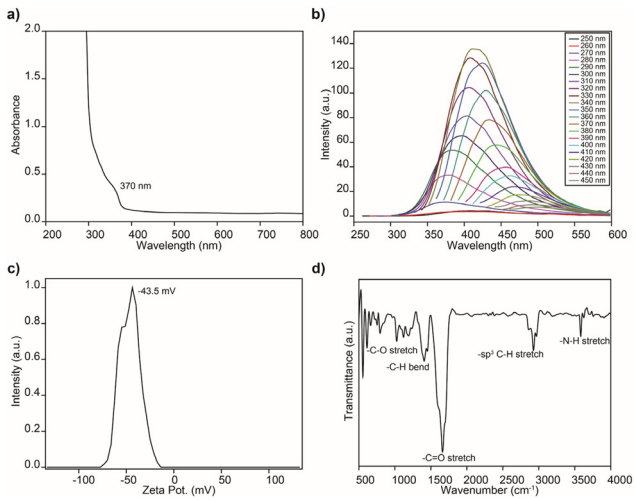

Fig. 2 Characterizations of CQDs: (a) UV-visible absorption spectrum; (b) excitation-dependent emission plot showing the polychromophoric nature of the nanomaterial; (c) zeta potential curve substantiating the exceptional stability of the nanomaterial and (d) FT-IR spectrum revealing the characteristic stretching and bending bands in the nanomaterial, retained from the L-cysteine precursor.

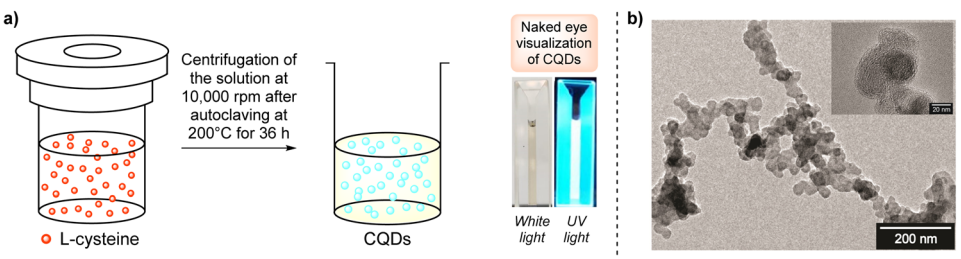

Fig. 1 (a) Hydrothermal approach for the synthesis of CQDs, and visual appearance of the as-prepared material in white light as well as UV light. (b) Microscopic characterization: TEM image of the as-prepared CQDs, showing the particles (inset: the network of spherical CQDs).

The surface charge for the CQDs was found to be −43.5 mV (Fig. 2c). Such a highly negative value of the zeta potential is indicative of the exceptional stability and non-aggregative nature of the CQDs, which is also evident from the fact that the as-prepared material retained its optical and microscopic properties even after several months. From the FT-IR (Fourier transform-infrared) spectrum, the CQDs were found to retain the functionalities present in the native form, such as the C–O/C═O, N–H stretches and the C–H bend (Fig. 2d).

XPS (X-ray photoelectron spectroscopy) was carried out to determine the elemental composition after undergoing hydrothermal treatment. The CQDs were found to retain the elemental composition of the precursor, L-cysteine (Fig. 3). The deconvolution of the S 2p spectrum confirmed the existence of S^- and the SH moiety, while the C 1s XPS plot was indicative of the singly bonded C–C, C–S, C–O, as well as C═O entities. Likewise, the existence of C–N and N–H bonds was clear in the N 1s spectrum. Additionally, the absence of the peak around 535 eV in the O 1s spectrum confirmed the absence of the C–O–H group, which implies that the carboxylic acid is converted to the carboxylate analogue. This further accounts for the negative zeta potential value.[55]

The quantum yield of the CQDs was measured using 7-hydroxyxoumarin as the reference (SI, section 5). The UV-visible and fluorescence spectra were recorded for the reference and samples in H_2O. Using this method, the quantum yield of CQDs was found to be 4.8%.

Following the preparation and characterization of the CQDs, we proceeded to explore the utility of the as-prepared nanomaterial for NKR.

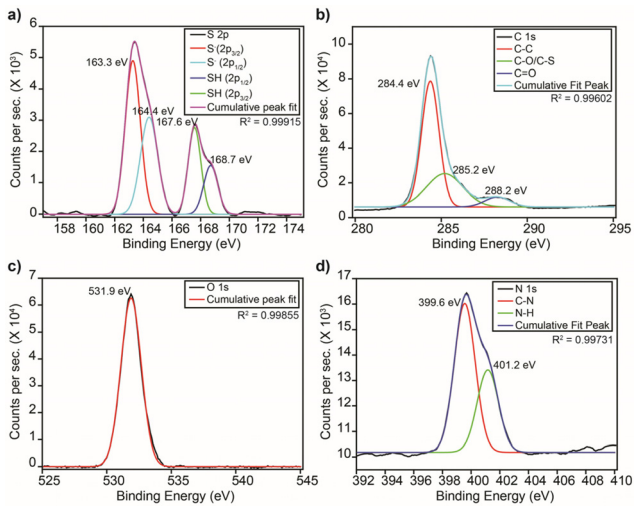

Fig. 3 Deconvoluted XPS plots of CQDs, confirming the elemental composition of the surface and the core: (a) S 2p; (b) C 1s; (c) O 1s and (d) N 1s.

Optimization and screening of the reaction conditions for NKR using CQDs

At the outset of our investigation, we employed *O*-(4-methoxyphenyl) dimethylcarbamothioate **1a** as the model substrate. In the case of intramolecular rearrangements, the substrate loading is very important, since high substrate loading can affect the kinetics of the process, while very low loading reduces the economy of the process. At 0.25 mmol loading of **1a**, we were delighted to observe the formation of the product *S*-(4-methoxyphenyl) dimethylcarbamothioate **2a**, albeit in very low yield (Table 1, entry 1). A reduction in the loading of **1a** enhanced the yield to some extent (Table 1, entry 2).

Subsequently, we screened various sources of light and found that irradiation with a blue LED of higher wattage (20 W) improved the yield to 44% (Table 1, entries 3 and 4). Using THF as the solvent did not help in further improving the output of the reaction (Table 1, entry 5).

Upon literature survey, we realized that the H_2O content in the reaction medium affected the overall yield of **2a**, since it resulted in the formation of the side product **2a′**, which is the oxidized analogue of the precursor/product, and is very commonly observed in the NKR process. However, the use of H_2O could not be completely ruled out from the reaction medium, since the catalyst was only soluble in H_2O. Therefore, we decided to screen the effect of the H_2O quantitatively. Indeed, upon reduction of the H_2O content, the yield of **2a** showed a significant enhancement (Table 1, entries 6–8). Standard blue LEDs (which are conventionally adopted for most of the photo-driven reactions) can also drive the reaction to a significant outcome (63%: Table 1, entry 8), albeit, in a much higher time scale.

When a Kessil Lamp (370 nm) was used as the source of irradiation, **2a** was formed in 98% yield in a time frame of just 1 h (Table 1, entry 9). Irradiation with a light source that excited the CQDs at a wavelength corresponding exactly to its absorption maxima resulted in such a drastic increment *via* enhanced efficacy of the catalyst, concomitantly reducing the time frame of the reaction significantly as well.

Furthermore, no side product (including **2a′**) was observed, highlighting the efficacy of the strategy, as evident from the NMR spectrum of the crude reaction mixture (SI, section 6).

Various control reactions highlighted the importance of a suitable light source (as well as the CQDs) for realising the optimal output of the NKR process (Table 1, entries 10–12). Using a dry solvent was also impetus for the strategy (Table 1, entry 13).

Importantly, NKR does not take place in the absence or presence of the catalyst even at elevated temperatures, which shows the importance of having such a strategy operating under ambient conditions (Table 1, entries 14 and 15).

In summary, the optimal parameters for the ambient temperature NKR corresponded to a reaction time of 1 h in dry MeCN solvent with a small loading of CQDs (0.68 mg or

Table 1 Optimization of NKR using CQDs

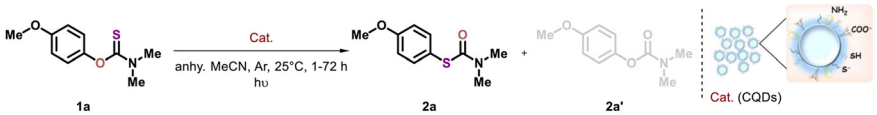

Entry	Light	Catalyst/H_2O content	Time (h)	NMR yield (%)
1[a]	Blue LED (10 W)	0.68 mg/200 μL	72	18
2	Blue LED (10 W)	0.68 mg/200 μL	72	34
3	CFL (45 W)	0.68 mg/200 μL	72	10
4	Blue LED (20 W)	0.68 mg/200 μL	72	44
5[b]	Blue LED (20 W)	0.68 mg/200 μL	72	26
6	Blue LED (20 W)	0.68 mg/300 μL	72	41
7	Blue LED (20 W)	0.68 mg/100 μL	72	54
8	Blue LED (20 W)	0.68 mg/50 μL	72	63
9	Kessil (370 nm)	0.68 mg/50 μL	1	98 (94)
10		0.68 mg/50 μL	1	n.d.
11	Kessil (370 nm)	—	1	Trace
12	—	—	1	n.d.
13[c]	Kessil (370 nm)	0.68 mg/50 μL	72	48
14[d]	—	—	72	n.d.
15[d]	—	0.68 mg/50 μL	72	n.d.

Reaction conditions: 0.125 mmol of *O*-(4-methoxyphenyl) dimethylcarbamothioate **1a** (except entry 1) was taken in a clean, dried reaction tube equipped with a magnetic stir-bar. The tube was degassed under the effect of vacuum and purged with Ar. 2 mL of anhydrous MeCN (distilled to dryness with P_2O_5 and stored over activated 4 Å MS) was added (except entries 5 and 13), followed by the addition of the catalyst (CQDs were used as an aqueous solution; the water content was adjusted as mentioned) (except entries 11, 12 and 14). The reaction tube was ultrasonicated (if required) and irradiated for the mentioned time using the stated light source (except entries 10, 12, 14 and 15) at 25 °C (except entries 14 and 15). The reaction mixture was subjected to an EtOAc/H_2O workup. The organic phase was analysed by ^{1}H-NMR, and the product **2a** was quantified using dibromomethane as the reference in $CDCl_3$ solvent for obtaining the NMR yield; for entry 9, the isolated yield is reported in parentheses. [a] 0.25 mmol of the substrate **1a** was used. [b] Dry THF was used as the solvent. [c] Regular MeCN was used. [d] The reaction temperature was kept at 50/100 °C. 0.68 mg of CQDs correspond to a weight percent of 2.5 (relative to the limiting reagent **1a**) and 50 μL H_2O corresponds to 2.5% v/v (relative to the total solvent volume). (n.d. = not determined; EtOAc: ethyl acetate, MeCN: acetonitrile).

0.0026 mol%, dispersed in 50 μL of H_2O), activated upon irradiation with a Kessil lamp.

Substrate scope: analysing the generality of the protocol

Post-optimization, the scope of the protocol was studied using a diverse array of substrates, *vide infra* (Scheme 2). In general, it was observed that substrates bearing electron-donating substituents on the aryl ring participated in the reaction more efficiently, giving moderate to excellent yields as compared to the substrates bearing electron-withdrawing substituents on the aryl ring.

When *O*-phenyl dimethylcarbamothioate **1b** was subjected to the optimal conditions, the yield of the derivative **2b** (Scheme 2) was found to be very low, which could be improved by doubling the catalyst loading. This was attributed to the absence of any activating effect which could arise *via* substituent incorporation.

The inclusion of one or two –OMe moieties in the *ortho* position results in the rearranged product in a time span of just 1 h (Scheme 2: derivatives **2c** and **2d**). The incorporation of the *tert*-butyl moiety in the *para* position also drives the reaction to a favourable outcome (Scheme 2: derivative **2e**), albeit, at a considerably longer time frame (48 h) due to the distal +I effect. This was also evident from the incorporation of two –Me groups at different positions of the aryl ring. Proximal –Me groups facilitated the rearranged product formation in a shorter time frame (10 h for substrate **1f** bearing the 2 –Me groups at the *ortho* positions), as compared to the cases where the –Me substitutions were done at distal sites or at the *meta* position of the aryl ring (Scheme 2: derivatives **2f**, **2g**, **2h** and **2i**).

The substrate bearing three –Me groups at the *ortho* and *para* positions was also well endured during the course of the reaction (Scheme 2: derivative **2j**), with a reaction time of just 5 h.

Other scaffolds such as the olefinic group, heteroatom bearing functionalities (*e.g.*, amides) and halogenated ring systems were compatible with the NKR reaction conditions (Scheme 2: derivatives **2k**, **2l**, **2m** and **2n**) with moderate reaction times (24–48 h).

Polyaromatic derivatives of *O*-aryl carbamothioates in the unsubstituted and halogenated forms could be subjected to NKR using CQDs as well (Scheme 2: derivatives **2o**, **2p** and **2q**).

A long-chain substituent was included at the *para* position of the aryl ring without affecting the reaction efficiency (Scheme 2: derivative **2r**). Furthermore, the replacement of two –Me groups with two –Et groups in the *O*-aryl carbamothioates furnished the rearranged product in appreciable outputs (Scheme 2: derivatives **2s**, **2t** and **2u**).

The generality of the protocol was evident from the fact that electronically rich/deficient and neutral substrates could be accommodated under ambient conditions in the current strategy, although the yields were dependent on the underlying mechanism operating in this case, further

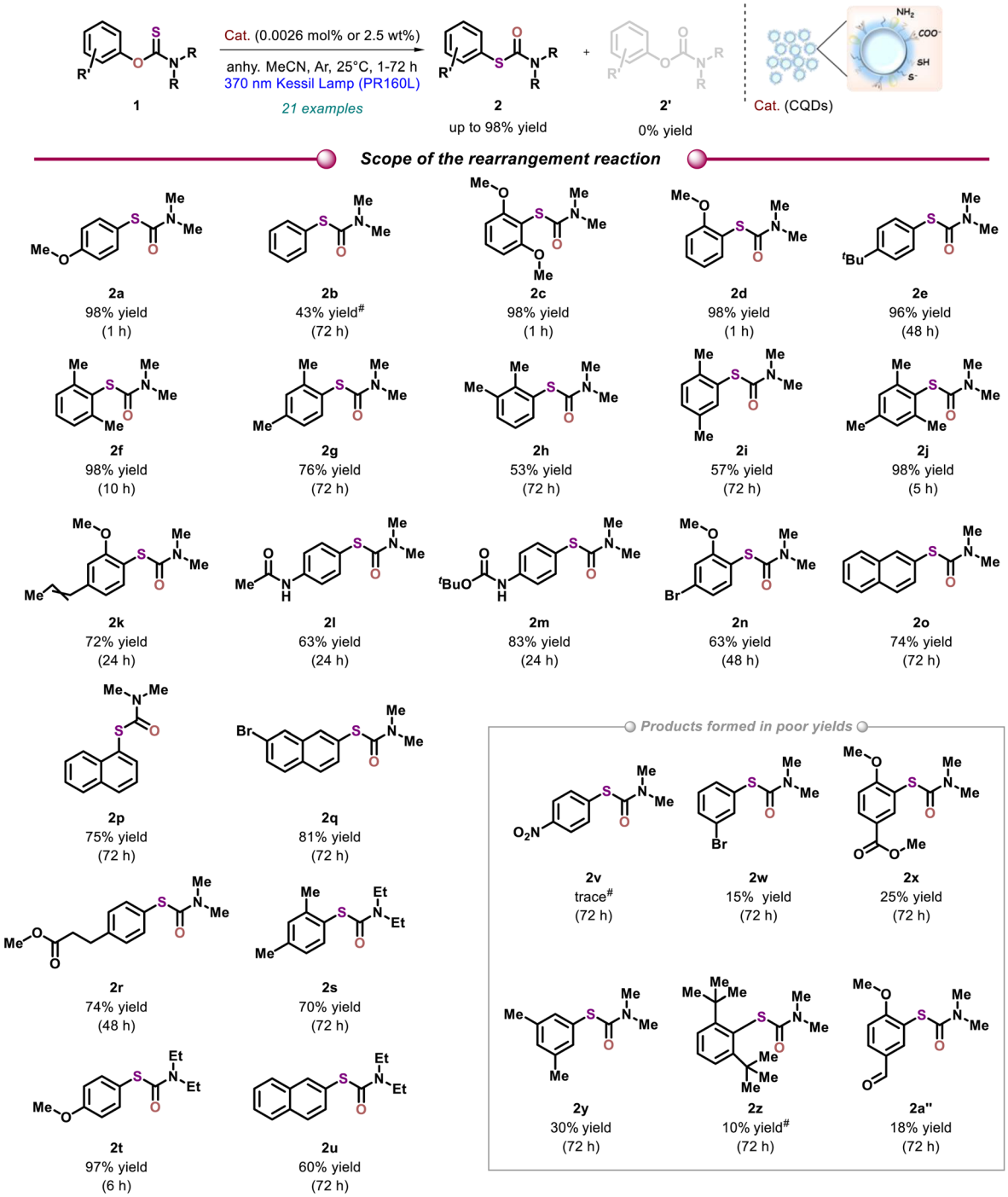

Scheme 2 Scope of the NKR reaction, photo-mediated by CQDs (isolated yields are reported in all cases except for the derivatives obtained in poor yield, *viz.*, **2v**–**2z**, **2a″**); #: catalyst loading was doubled.

providing a scope for subsequent investigations in this field.

The substrates which did not participate efficiently in the reaction gave us a subtle lead for the mechanism driving NKR in our case. For instance, substrates having an electron-withdrawing group in the aryl ring (Scheme 2: derivatives **2v**, **2w**, **2x** and **2a″**) or electron-donating groups (*via* +I effect), but in the *meta* position (Scheme 2: derivative **2y**), did not furnish the desired product in appreciable yields. Analogously, the derivatives with cyano or ester functionalities in the aryl rings did not participate efficiently in the reaction, giving trace products (<10%) even after 48 h of irradiation. Additionally, the reaction did not work for sterically encumbered substrates, such as those bearing *tert*-butyl substituents in the *ortho* position

(Scheme 2: derivative **2z**) even at longer reaction times (72 h). In these cases, the steric factor overwhelms the rotational restriction around the Ar–O bond caused by the smaller substituents at the *ortho* position.

Scalability of the protocol and recyclability of CQDs

We also analysed the scalability of the reaction by taking 0.25 mmol and 0.625 mmol of **1a** (scale-up factor = 2 and 5, respectively). The yield of **2a** was found to be 75% and 48% (NMR yield), respectively. The loss in yield was attributed to the collisional quenching and aggregation of the QDs at higher loadings, further considering the intramolecular nature of the NKR reaction. This limitation can be overcome by using flow chemistry as reported earlier,[9] which is beyond the scope of the present study.

In order to check the heterogeneous nature of the catalyst, reusability studies were conducted. One of the important advantages of heterogeneous catalysts is their ability to retain the efficacy in subsequent runs of the reaction. Thus, the CQDs were separated from the reaction mixture (using a workup with EtOAc/H_2O) and reused for the successive cycles of NKR of **1a**, subjected to the optimized condition. The NMR yield of the desired product **2a** was determined at the end of each cycle.

The reusability was carried out for up to ten cycles, and the CQDs were found to retain their activity in all of the runs (Fig. 4), further establishing the heterogeneity of the catalyst. The network morphology and optical properties (absorption profile) of the CQDs were also found to remain intact even after being subjected to multiple runs (SI, section 8).

Mechanistic investigations

In order to understand the mechanism of the CQD-mediated NKR, we inducted various quenchers in the reaction medium (Schemes 3 and 4).

The decrease in the yields of the reaction upon the use of Na_2CrO_4 and DIPEA (*N*,*N*-diisopropylethylamine) confirms the involvement of electrons and holes in the catalytic cycle

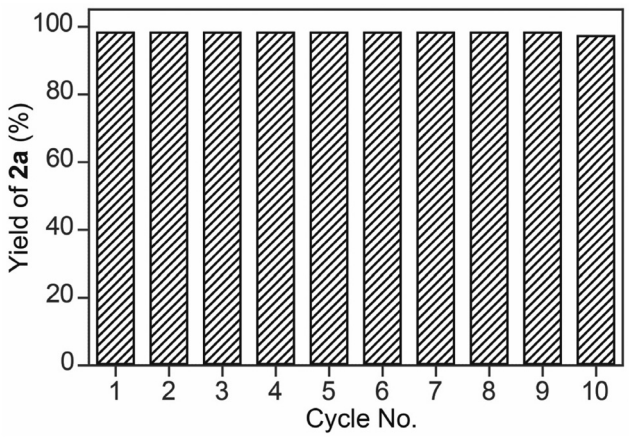

Fig. 4 Recyclability of CQDs in the NKR reaction leading to **2a** from **1a**.

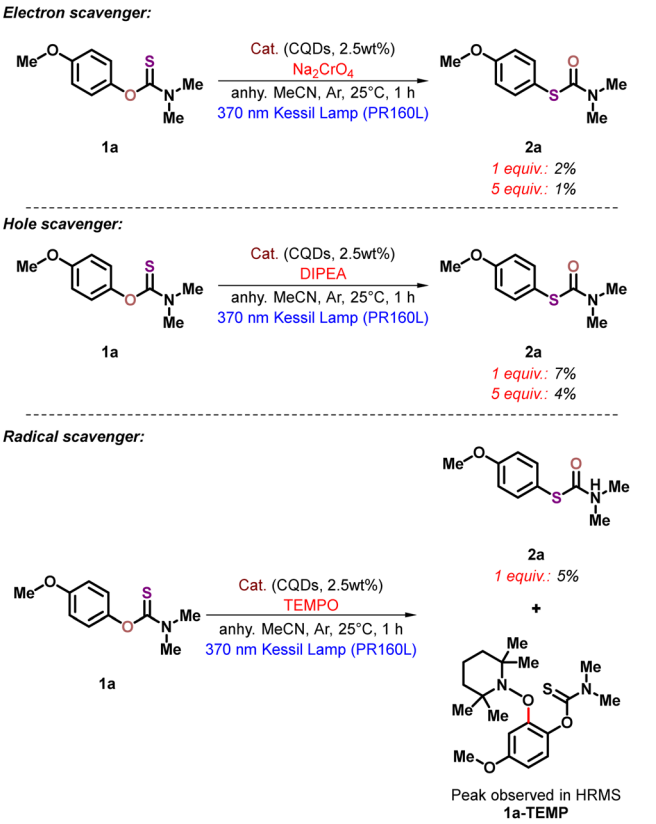

Scheme 3 Impact of various quenchers on the NKR of **1a**, confirming the operation of a single electron transfer (SET) mechanism (NMR yields are reported).

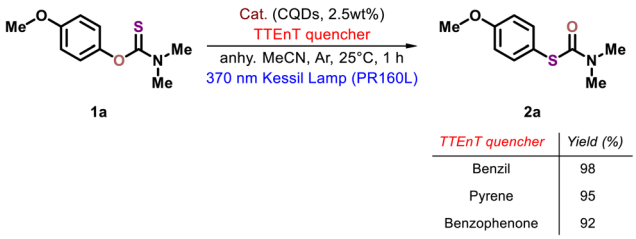

TTEnT quencher	Yield (%)
Benzil	98
Pyrene	95
Benzophenone	92

Scheme 4 Impact of various TTEnT quenchers on the NKR of **1a**, confirming the absence of an energy transfer mechanism (NMR yields have been reported).

(Scheme 3, top and middle). The electron scavenger, Na_2CrO_4 prevents the transfer of electrons from the *O*-aryl carbamothioates **1** to the CQDs. In contrast, DIPEA is capable of quenching the hole in the valence band (VB). This implies that photoirradiation generates the exciton in the CQDs. A sharp decline in the yield was also observed upon the use of TEMPO (2,2,6,6-tetramethyl-1-piperidinyloxy) (Scheme 3, bottom). This was attributed to the formation of the intermediate **1a-TEMP** (confirmed by HRMS (ESI+)). Since the formation of the desired intermediate/TS is blocked in the presence of TEMPO, the yield decreases. These results confirm the involvement of a HET (heterogeneous electron transfer) process.

Additionally, we investigated the possibility of energy transfer processes in the reaction mechanism using various related quenchers such as benzil, pyrene and benzophenone (Scheme 4). These are known to be quenchers of the triplet excited state, mainly *via* Dexter energy transfer mechanisms. Such energy transfer processes are common for CdSe and CdS QDs.[56] However, in the case of the CQDs, the yield did not differ significantly as compared to the optimal output, which substantiated the absence of any triplet-to-triplet energy transfer (TTEnT) process. Both CQDs and light are quintessential to realizing the optimal output of the NKR process, as already demonstrated in Table 1.

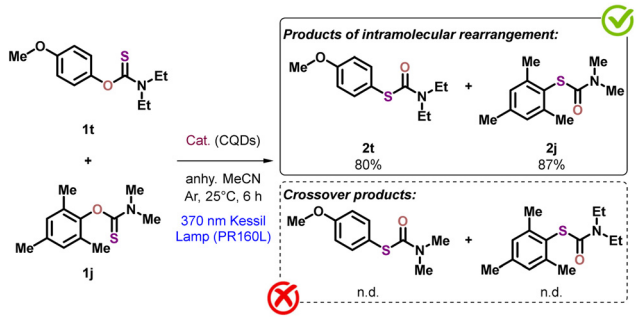

Scheme 5 Crossover experiments to check for the possibility of intermolecular *vs.* intramolecular routes in the CQD-mediated NKR process.

The electron transfer abilities of the CQDs corroborated with the CV studies, which further confirmed the involvement of the CQDs in a HET process (Fig. 5). For the purpose of the potentiodynamic electrochemical measurements, the ferrocyanide–ferricyanide couple (sensitive to the electrode surface) was taken, while KCl served the purpose of an electrolyte. ΔE_p (the peak-to-peak separation between the anodic and cathodic peak) decreases when the rate of HET is enhanced upon the addition of a suitable species, resulting in improved catalytic properties as compared to other nanomaterials.[49,57]

The Stern–Volmer experiment revealed the effective interaction between the CQDs and **1a** *via* a drop in the fluorescence intensity of the photocatalyst upon the addition of **1a** in successively increasing amounts. The Stern–Volmer quenching constant was found to be 54.43 (SI, section 7), as per the following equation:

$$\frac{I_0}{I} = 1 + K_{SV}[Q]$$

where: I_0 = Fluorescence intensity of the CQDs; I = Fluorescence intensity of the CQDs upon the addition of the quencher Q (in this case, **1a**); K_{SV} = Stern–Volmer constant; [Q] = Concentration of the quencher Q (in this case, **1a**).

In order to establish the intramolecular nature of NKR reaction, crossover experiments were done using **1t** and **1j**, subjected to the optimal reaction conditions. No crossover pro-

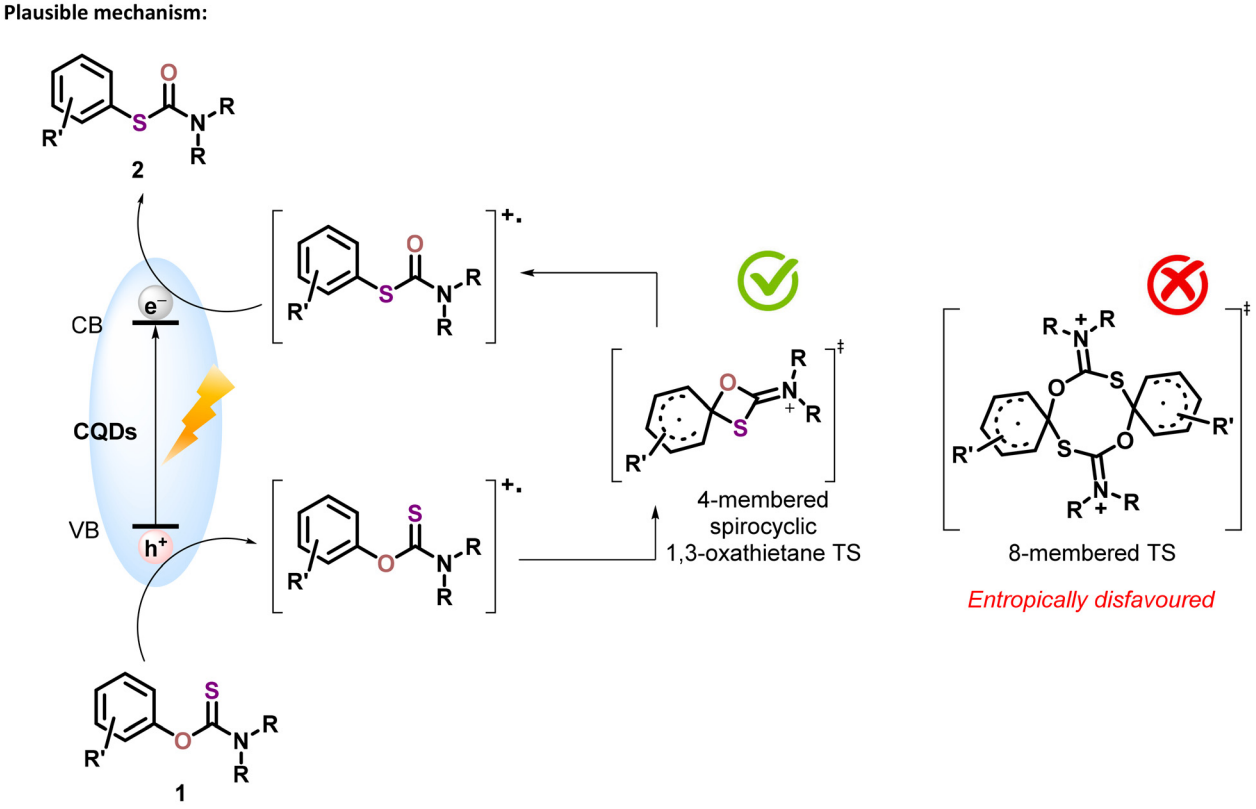

Scheme 6 Plausible mechanism for the NKR of *O*-aryl carbamothioate **1** to *S*-aryl carbamothioate **2** using CQDs as the photocatalyst.

ducts were detected, which rules out the operation of an intermolecular rearrangement process (Scheme 5).

Based on the results discussed above and the literature precedence, we propose the plausible mechanistic pathway for the CQDs photocatalyst-mediated NKR (Scheme 6). The photoirradiation of the CQDs results in the generation of an exciton in the nanomaterial. The ground state of the photocatalyst is regenerated by the *O*-aryl carbamothioate **1**, which is also evident from the fact that electronically rich substrates are more facile participants in NKR, as obvious from the scope of the reaction. The *O*-aryl carbamothioate subsequently forms the radical cation, which proceeds to generate the four-membered spirocyclic 1,3-oxathietane TS. At higher substrate concentrations, an eight-membered bimolecular cyclic TS may also be formed, when two such substrate moieties come together.[48,58,59] However, the results of the crossover experiments invariably prove that such a bimolecular TS is not formed. Moreover, the generation of such a TS is entropically disfavoured. The oxathietane TS, being unstable, breaks to generate the thermodynamically more stable *S*-aryl carbamothioate radical cation. This will take the electron from the conduction band (CB) of the CQDs to furnish the final product **2**, thereby completing the catalytic cycle.

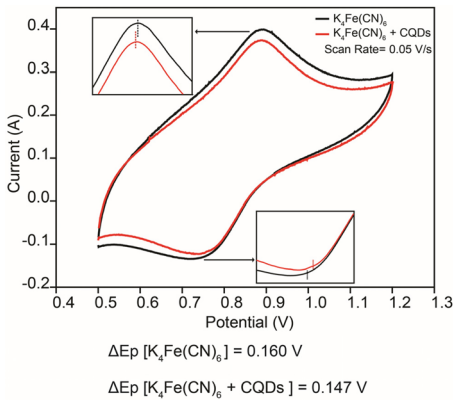

Fig. 5 Cyclic voltammograms showing the involvement of CQDs in the HET process.

Evaluation of green chemistry metrics for the CQDs photomediated NKR

An assessment of the metrics typically associated with green chemistry is imperative to realising how efficient and sustainable the protocol is. In this regard, we have estimated several parameters (as shown in Table 2).[60]

These values clearly highlight the efficient and benign nature of the protocol in terms of minimal waste generation (low *E*-factor; close to 0 ideally). While the AE is indicative of the efficacy of the reaction design, the actual stoichiometry and the yield is considered during the calculation of the RME, which, herein, proves the high consumption of the reactant driven towards the formation of the desired product. The OE value indicates that the 'ideal' design and practical execution of the reaction are close to one another, justifying its viability.

Energetically, the scheme is efficient and does not require the use of high temperatures or hazardous conditions to be executed. As explained in the introduction, the EcoScale score of 83 highlights the efficiency, sustainability and simple *modus operandi* for the aforesaid strategy (SI, section 9).

Conclusions

Taking another step towards expanding the regime of heterogeneous nanomaterial-based photocatalysis, CQDs were tailored from the naturally-occurring amino acid L-cysteine using a facile hydrothermal approach without inducting any capping agent or stabilizer. The nanodots were subsequently used for

Table 2 Estimation of the green chemistry metrics for the CQD-mediated NKR driven by light

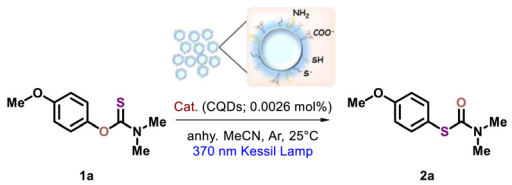

Parameter	Formula	Value
Environmental factor (*E*-factor)	$\frac{\text{Mass of waste}}{\text{Mass of isolated product}}$	0.02
Reaction mass efficiency (RME)	$\frac{\text{Mass of isolated product}}{\sum \text{Mass of reactants stoichiometrically}} \times 100$	97.99%
Atom economy (AE)	$\frac{\text{Molecular weight of product (s)}}{\sum \text{Molecular weight of reactant (s)}} \times 100$	100%
Optimum efficiency (OE)	$\frac{\text{RME}}{\text{AE}} \times 100$	97.99%

ambient temperature NKR, thereby providing access to a broad range of electronically diverse *S*-aryl carbamothioates *via* a benign and sustainable strategy. The intramolecular rearrangement was proposed to proceed through a radical cationic oxathietane TS, formed *via* a SET process. The CQDs retained their activity in subsequent runs, demonstrating the robust nature of the as-prepared nanomaterial. This work highlights the advantages and the need for the rational/strategic design of nanomaterials to serve as potential catalysts in complex or critical synthetic strategies, paving the way for further development in this field, particularly with regard to the fabrication of common heterogeneous catalytic platforms that can operate in organic solvents for the transformation of electronically rich/deficient/neutral substrates. The reaction design and optimisation further excel as per the estimation of the metrics typically considered in green chemistry, justifying its sustainable and benign nature.

Experimental

General considerations

Detailed methods can be found in the SI, section 1.

Instrumentation

Detailed methods can be found in the SI, section 2.

Initial attempt for photocatalytic NKR

Detailed methods can be found in the SI, section 3.

Synthesis of cysteine-based CQDs

The CQDs were prepared using a hydrothermal approach, taking L-cysteine as the precursor. A solution of 0.32 g of L-cysteine dispersed in 32 mL of H_2O (*via* ultra-sonication) was transferred to Teflon-lined autoclave chambers. The setup was kept for 36 h at 200 °C. After cooling to room temperature, the solution was centrifuged for 30 min at 10 000 rpm. The supernatant was carefully retrieved and stored at 4 °C. The concentration was determined by lyophilization. The synthesized CQDs were sticky in nature after water removal.

Procedure for optical/microscopic characterization and sample preparation

Detailed methods can be found in the SI, section 4.1.

Characterization of CQDs

Details available in the SI, section 4.2.

Calculation of the molecular weight for the CQDs

Detailed methods can be found in the SI, section 4.3.

Procedure for the preparation of substrates

Detailed methods can be found in the SI, section 4.4.

General procedure for NKR

A clean, dried reaction tube equipped with a magnetic stir-bar was taken and cooled under the effect of Ar flow. 0.125 mmol of the *O*-aryl carbamothioate **1** was taken in the reaction tube. The tube was sealed with a septum and degassed under the effect of vacuum, followed by purging with Ar. The CQDs (2.5 wt% relative to **1**, dissolved in 50 μL of H_2O) along with 2 mL of anhydrous MeCN (distilled to dryness with P_2O_5 and stored over activated 4 Å MS) were added. The reaction mixture was ultra-sonicated (if required) and subsequently irradiated for the stated time using a Kessil Lamp (370 nm, PR160L). After the irradiation, the reaction mixture may be extracted with EtOAc (3 × 10 mL) (removal of MeCN under reduced pressure is sufficient otherwise). The combined organic phases were washed with brine and dried over anhydrous sodium sulphate. The solvent was removed by rotary evaporation. The rearranged product **2** was purified on a silica gel column (100–200 mesh) with EtOAc/hexane as the eluent.

For scaling up the reaction, the substrate and catalyst was loaded as per the scaling factors. The other conditions were maintained as per the optimized parameters.

For the control experiments, quenchers were added in suitable proportions wherever mentioned.

The NMR yield could be determined wherever required, using ^{1}H-NMR with dibromomethane as the reference in $CDCl_3$ solvent.

General procedure for the recyclability studies

After completion, the reaction mixture was concentrated to remove MeCN and subjected to work-up with EtOAc/H_2O mixture. The aqueous layer containing the catalyst was collected carefully. Any excess H_2O added during the work-up could be removed by lyophilization such that the residual catalyst remains suspended in 50 μL H_2O. **1a** was further added and the reaction vessel was subjected to the optimal reaction conditions. The studies were done for a total of 10 cycles and the NMR yields were reported in each case, using ^{1}H-NMR with dibromomethane as the reference in the $CDCl_3$ solvent.

General procedure for the cyclic voltammetry (CV) studies

Detailed methods can be found in the SI, section 4.5.

General procedure for the crossover experiments

Detailed methods can be found in the SI, section 4.6.

Measurement of quantum yield

Detailed methods can be found in the SI, section 5.

Spectra of the crude reaction mixture

Detailed spectra can be found in the SI, section 6.

General procedure for the Stern–Volmer quenching analysis

Stern–Volmer quenching experiments were done while keeping the catalyst and solvent concentration intact, as per the optimal conditions. The concentration of **1a** was varied

sequentially and the emission profile of the catalyst CQDs was monitored at an excitation wavelength of 370 nm.

Detailed plots can be found in the SI, section 7.

General procedure for the estimation of the EcoScale value

Detailed methods can be found in the SI, section 9.

Characterization data and NMR spectra

Detailed data can be found in the SI, sections 10 and 11.

Author contributions

K. J.: conceptualization, methodology development, experimentation, data analysis, manuscript preparation; M. M.: experimentation, data analysis, inputs during manuscript preparation; M. D.: conceptualization, data analysis, manuscript preparation, funding acquisition.

Conflicts of interest

An Indian patent has been filed for this work (application no. 202541045324, dated May 10, 2025). A previous version of this manuscript has been deposited on a preprint server (https://doi.org/10.26434/chemrxiv-2025-zjvrv). There are no other conflicts to declare.

Data availability

The data supporting this article have been included as part of the supplementary information (SI). Supplementary information is available. See DOI: https://doi.org/10.1039/d5gc05720e.

Acknowledgements

The authors would like to thank SERB (Science and Engineering Research Board, India) CRG/2020/001197 and DST-FIST (SR/FST/CSII-040/2015) for the financial/infrastructural support. K. J. thanks MHRD-PMRF for the doctoral fellowship, IISc for the infrastructural support and Mr Sarvesh from MRC, IISc, for helping in the setup for CV studies.

References

1 M. S. Newman and H. A. Karnes, *J. Org. Chem.*, 1966, **31**, 3980–3984.
2 G. C. Lloyd-Jones, J. D. Moseley and J. S. Renny, *Synthesis*, 2008, 661–689.
3 H. Jacobsen and J. P. Donahue, *Can. J. Chem.*, 2006, **84**, 1567–1574.
4 H. M. Relles and G. Pizzolato, *J. Org. Chem.*, 1968, **33**, 2249–2253.
5 K. Miyazaki, *Tetrahedron Lett.*, 1968, **9**, 2793–2798.
6 A. Kaji, Y. Araki and K. Miyazaki, *Bull. Chem. Soc. Jpn.*, 2006, **44**, 1393–1399.
7 J. D. Moseley, R. F. Sankey, O. N. Tang and J. P. Gilday, *Tetrahedron*, 2006, **62**, 4685–4689.
8 J. N. Harvey, J. Jover, G. C. Lloyd-Jones, J. D. Moseley, P. Murray and J. S. Renny, *Angew. Chem., Int. Ed.*, 2009, **48**, 7612–7615.
9 A. J. Perkowski, C. L. Cruz and D. A. Nicewicz, *J. Am. Chem. Soc.*, 2015, **137**, 15684–15687.
10 S. Prabhakar, P. Kar, S. P. Mirza, V. V. S. Lakshmi, K. Nagaiah and M. Vairamani, *Rapid Commun. Mass Spectrom.*, 2001, **15**, 2127–2134.
11 M. E. Matter, L. Čamdžić and E. E. Stache, *Angew. Chem., Int. Ed.*, 2023, **62**, e202308648.
12 P. Enders, K. Prane, E. Schönke, T. Taeufer, D. Michalik, J. Rabeah and R. Francke, *ChemCatChem*, 2023, **15**, e202300744.
13 K. D. Patel, R. K. Singh and H.-W. Kim, *Mater. Horiz.*, 2019, **6**, 434–469.
14 O. S. Ayanda, A. O. Mmuoegbulam, O. Okezie, N. I. Durumin Iya, S. a. E. Mohammed, P. H. James, A. B. Muhammad, A. A. Unimke, S. A. Alim, S. M. Yahaya, A. Ojo, T. O. Adaramoye, S. K. Ekundayo, A. Abdullahi and H. Badamasi, *J. Nanopart. Res.*, 2024, **26**, 106.
15 Q. Liu, L. Wei, J. Wang, F. Peng, D. Luo, R. Cui, Y. Niu, X. Qin, Y. Liu, H. Sun, J. Yang and Y. Li, *Nanoscale*, 2012, **4**, 7084–7089.
16 K. S. Novoselov, A. K. Geim, S. V. Morozov, D. Jiang, M. I. Katsnelson, I. V. Grigorieva, S. V. Dubonos and A. A. Firsov, *Nature*, 2005, **438**, 197–200.
17 K. S. Novoselov, A. K. Geim, S. V. Morozov, D. Jiang, Y. Zhang, S. V. Dubonos, I. V. Grigorieva and A. A. Firsov, *Science*, 2004, **306**, 666–669.
18 E. Perevedentseva, Y.-C. Lin, M. Jani and C.-L. Cheng, *Nanomedicine*, 2013, **8**, 2041–2060.
19 D. Tasis, N. Tagmatarchis, A. Bianco and M. Prato, *Chem. Rev.*, 2006, **106**, 1105–1136.
20 J. Liu, R. Li and B. Yang, *ACS Cent. Sci.*, 2020, **6**, 2179–2195.
21 J. Peng, W. Gao, B. K. Gupta, Z. Liu, R. Romero-Aburto, L. Ge, L. Song, L. B. Alemany, X. Zhan, G. Gao, S. A. Vithayathil, B. A. Kaipparettu, A. A. Marti, T. Hayashi, J.-J. Zhu and P. M. Ajayan, *Nano Lett.*, 2012, **12**, 844–849.
22 D. Pan, J. Zhang, Z. Li and M. Wu, *Adv. Mater.*, 2010, **22**, 734–738.
23 F. Yuan, T. Yuan, L. Sui, Z. Wang, Z. Xi, Y. Li, X. Li, L. Fan, Z. a. Tan, A. Chen, M. Jin and S. Yang, *Nat. Commun.*, 2018, **9**, 2249.
24 S. Zhu, Y. Song, X. Zhao, J. Shao, J. Zhang and B. Yang, *Nano Res.*, 2015, **8**, 355–381.
25 S. Lu, L. Sui, J. Liu, S. Zhu, A. Chen, M. Jin and B. Yang, *Adv. Mater.*, 2017, **29**, 1603443.
26 S. Zhu, Q. Meng, L. Wang, J. Zhang, Y. Song, H. Jin, K. Zhang, H. Sun, H. Wang and B. Yang, *Angew. Chem., Int. Ed.*, 2013, **52**, 3953–3957.

27 J. Liu, Y. Geng, D. Li, H. Yao, Z. Huo, Y. Li, K. Zhang, S. Zhu, H. Wei, W. Xu, J. Jiang and B. Yang, *Adv. Mater.*, 2020, **32**, 1906641.
28 F. Yuan, Z. Wang, X. Li, Y. Li, Z. a. Tan, L. Fan and S. Yang, *Adv. Mater.*, 2017, **29**, 1604436.
29 S. Qu, D. Zhou, D. Li, W. Ji, P. Jing, D. Han, L. Liu, H. Zeng and D. Shen, *Adv. Mater.*, 2016, **28**, 3516–3521.
30 T. Gao, X. Wang, L.-Y. Yang, H. He, X.-X. Ba, J. Zhao, F.-L. Jiang and Y. Liu, *ACS Appl. Mater. Interfaces*, 2017, **9**, 24846–24856.
31 K. Jiang, S. Hu, Y. Wang, Z. Li and H. Lin, *Small*, 2020, **16**, 2001909.
32 Q. Su, C. Lu and X. Yang, *Carbon*, 2019, **152**, 609–615.
33 K. Jiang, Y. Wang, Z. Li and H. Lin, *Mater. Chem. Front.*, 2020, **4**, 386–399.
34 S. Tao, S. Lu, Y. Geng, S. Zhu, S. A. T. Redfern, Y. Song, T. Feng, W. Xu and B. Yang, *Nat. Commun.*, 2018, **57**, 2393–2398.
35 X. Zhao, Q. Tang, S. Zhu, W. Bu, M. Yang, X. Liu, Y. Meng, W. Yu, H. Sun and B. Yang, *Nanoscale*, 2019, **11**, 9526–9532.
36 T. Fan, G. Zhang, L. Jian, I. Murtaza, H. Meng, Y. Liu and Y. Min, *J. Alloys Compd.*, 2019, **792**, 844–850.
37 Y. Han, D. Tang, Y. Yang, C. Li, W. Kong, H. Huang, Y. Liu and Z. Kang, *Nanoscale*, 2015, **7**, 5955–5962.
38 S. Bhattacharyya, F. Ehrat, P. Urban, R. Teves, R. Wyrwich, M. Döblinger, J. Feldmann, A. S. Urban and J. K. Stolarczyk, *Nat. Commun.*, 2017, **8**, 1401.
39 D. Sarma, B. Majumdar and T. K. Sarma, *Green Chem.*, 2019, **21**, 6717–6726.
40 F. Wang, Y.-h. Chen, C.-y. Liu and D.-g. Ma, *Chem. Commun.*, 2011, **47**, 3502–3504.
41 H. Bian, Q. Wang, S. Yang, C. Yan, H. Wang, L. Liang, Z. Jin, sG. Wang and S. Liu, *J. Mater. Chem. A*, 2019, **7**, 5740–5747.
42 C. Zheng, N. Luo, S. Huang, W. Wu, H. Huang and M. Wei, *ACS Sustainable Chem. Eng.*, 2019, **7**, 10198–10206.
43 F. Lin, C. Li, L. Dong, D. Fu and Z. Chen, *Nanoscale*, 2017, **9**, 9056–9064.
44 D.-W. Zheng, B. Li, C.-X. Li, J.-X. Fan, Q. Lei, C. Li, Z. Xu and X.-Z. Zhang, *ACS Nano*, 2016, **10**, 8715–8722.
45 S.-Y. Sung, Y.-L. Su, W. Cheng, P.-F. Hu, C.-S. Chiang, W.-T. Chen and S.-H. Hu, *Nano Lett.*, 2019, **19**, 69–81.
46 A. Selim, R. Sharma, S. M. Arumugam, S. Elumalai and G. Jayamurugan, *ChemistrySelect*, 2022, **7**, e202104448.
47 R. Sharma, A. Selim, B. Devi, S. M. Arumugam, S. Sartaliya, S. Elumalai and G. Jayamurugan, *Biomass Convers Biorefin.*, 2024, **14**, 11445–11457.
48 K. Jaiswal, Y. R. Girish, P. Behera and M. De, *ACS Org. Inorg. Au*, 2022, **2**, 205–213.
49 K. Jaiswal, Y. R. Girish and M. De, *ACS Appl. Nano Mater.*, 2020, **3**, 84–93.
50 Y. R. Girish, K. Jaiswal, P. Prakash and M. De, *Catal. Sci. Technol.*, 2019, **9**, 1201–1207.
51 K. Jaiswal, K. Roy and M. De, *ACS Appl. Mater. Interfaces*, 2025, **17**, 35585–35596.
52 K. Jaiswal, R. Jagtap and M. De, *Nanoscale*, 2025, **17**, 13746–13755.
53 A. Bardow, J. Pérez-Ramírez, S. Sala and L. Vaccaro, *Green Chem.*, 2024, **26**, 11016–11018.
54 K. Van Aken, L. Strekowski and L. Patiny, *Beilstein J. Org. Chem.*, 2006, **2**, 3.
55 D. Wang, W. U. Khan, Z. Tang and Y. Wang, *Chem. – Asian J.*, 2018, **13**, 292–298.
56 J. P. Deore and M. De, *J. Org. Chem.*, 2023, **88**, 16292–16301.
57 N. Rohaizad, C. C. Mayorga-Martinez, Z. Sofer and M. Pumera, *ACS Appl. Mater. Interfaces*, 2017, **9**, 40697–40706.
58 J. P. Gilday, P. Lenden, J. D. Moseley and B. G. Cox, *J. Org. Chem.*, 2008, **73**, 3130–3134.
59 M. Burns, G. C. Lloyd-Jones, J. D. Moseley and J. S. Renny, *J. Org. Chem.*, 2010, **75**, 6347–6353.
60 K. Jaiswal, K. Roy and M. De, *ACS Appl. Mater. Interfaces*, 2025, **17**, 35585–35596.

